Eur. J. Mineral., 34, 411–424, 2022
https://doi.org/10.5194/ejm-34-411-2022

European Journal of Mineralogy
Open Access

Melting relations of Ca–Mg carbonates and trace element signature of carbonate melts up to 9 GPa – a proxy for melting of carbonated mantle lithologies

Melanie J. Sieber[1,a], Max Wilke[2], Oona Appelt[1], Marcus Oelze[1,b], and Monika Koch-Müller[1]

[1]Section 3.6 and 3.1, GFZ German Research Centre for Geosciences, Telegrafenberg, 14473 Potsdam, Germany
[2]Mineralogy, Institute of Geosciences, University of Potsdam,
Karl-Liebknecht-Straße 24–25, 14476 Potsdam, Germany
[a]present address: Mineralogy, Institute of Geosciences, University of Potsdam,
Karl-Liebknecht-Straße 24–25, 14476 Potsdam, Germany
[b]present address: Bundesanstalt für Materialforschung und -prüfung (BAM),
Richard-Willstätter-Straße 11, 12489 Berlin, Germany

Correspondence: Melanie J. Sieber (sieber.m.j@gmail.com)

Received: 2 March 2022 – Revised: 15 August 2022 – Accepted: 26 August 2022 – Published: 6 October 2022

Abstract. The most profound consequences of the presence of Ca–Mg carbonates ($CaCO_3$–$MgCO_3$) in the Earth's upper mantle may be to lower the melting temperatures of the mantle and control the melt composition. Low-degree partial melting of a carbonate-bearing mantle produces CO_2-rich, silica-poor melts compositionally imposed by the melting relations of carbonates. Thus, understanding the melting relations in the $CaCO_3$–$MgCO_3$ system facilitates the interpretation of natural carbonate-bearing silicate systems.

We report the melting relations of the $CaCO_3$–$MgCO_3$ system and the partition coefficient of trace elements between carbonates and carbonate melt from experiments at high pressure (6 and 9 GPa) and temperature (1300–1800 °C) using a rocking multi-anvil press. In the absence of water, Ca–Mg carbonates are stable along geothermal gradients typical of subducting slabs. Ca–Mg carbonates ($\sim Mg_{0.1–0.9}Ca_{0.9–0.1}CO_3$) partially melt beneath mid-ocean ridges and in plume settings. Ca–Mg carbonates melt incongruently, forming periclase crystals and carbonate melt between 4 and 9 GPa. Furthermore, we show that the rare earth element (REE) signature of Group-I kimberlites, namely strong REE fractionation and depletion of heavy REE relative to the primitive mantle, is resembled by carbonate melt in equilibrium with Ca-bearing magnesite and periclase at 6 and 9 GPa. This suggests that the dolomite–magnesite join of the $CaCO_3$–$MgCO_3$ system might be useful to approximate the REE signature of carbonate-rich melts parental to kimberlites.

Highlights.

- We report the melting relations of Ca–Mg carbonates in the upper mantle up to 9 GPa.
- Between 4 and 9 GPa, Ca–Mg carbonates melt incongruently, producing periclase.
- Carbonate–melt partitioning coefficients are established.

1 Introduction

Ca–Mg carbonates in the Earth's mantle are present in spinel-peridotite xenoliths (1 GPa) (Ionov et al., 1993), as inclusions in olivine from leucitite lava flows (~ 3–4 GPa) (Humphreys et al., 2010), in high-pressure calc–silicate rocks (4.5–7.5 GPa) (Korsakov and Hermann, 2006; Shatsky et al., 2006) and as inclusions in kimberlitic diamonds (Zedgenizov et al., 2014; Brenker et al., 2007; Wang et al., 1996). Experimental studies have shown that carbonates are stable in the subsolidus phase in locally oxidized zones of the up-

per mantle. For example, dolomite is stable up to 3 GPa in anhydrous peridotite assemblages (Falloon and Green, 1989) and Ca-rich carbonates are stable in eclogitic assemblages (Yaxley and Brey, 2004; Yaxley and Green, 1994). With increasing pressure (P), magnesite is likely to become the dominant carbonate species because Ca and Fe are preferentially incorporated into mantle silicate minerals (Dasgupta and Hirschmann, 2006).

The presence of solid carbonates with specific chemical composition in the mantle may initiate partial melting and influences the composition of CO_2-rich magmas formed by very low-degree partial melting of carbonated eclogites and carbonated peridotites (e.g., Hammouda and Keshav, 2015; Yaxley et al., 2019, and references therein). Carbonate melts form in a variety of tectonic settings, including subduction zones beneath volcanic arcs, in the upwelling carbonaceous mantle beneath mid-ocean ridges, beneath ocean islands in intraplate environments and in the cratonic lithospheric mantle (summarized in Yaxley et al., 2019). Despite the tectonic setting, the presence of carbonates reduces the solidus of peridotite by about 350–480 °C at 6 GPa, and the near-solidus melts of carbonated peridotite and carbonated eclogite are dolomitic with enrichments in Na_2O and K_2O (Ghosh et al., 2009; Wallace and Green, 1988; Dasgupta and Hirschmann, 2010, 2006; Dalton and Presnall, 1998). Because of the very small fractions of CO_2-rich melts, accurately determining the chemical composition of near-solidus melts is problematic in experimental studies, and mass balance calculations are subject to large uncertainties. The situation is even more profound for the trace element composition of initial CO_2-rich melts, and few studies have reported the trace element composition of near-solidus melts from high pressures ($\geq$ 6 GPa) (Brey et al., 2007; Dasgupta et al., 2009).

Allowing detailed understanding of the subsolidus and melting relations, minimum melting temperature (T), and chemical composition of initial carbonate melts, experimental studies have established the phase and melting relations of the K-, Na-, Fe-, Mg- and Ca-carbonate systems (e.g., Litasov, 2011; Shatskiy et al., 2016, 2013; Müller et al., 2017; Buob, 2006). Melting and phase relations are known up to 6 GPa for Ca–Mg carbonates (Sieber et al., 2020, and references therein). The melting curve of end-member $MgCO_3$ is constrained between 2.7 and 6 GPa (Irving and Wyllie, 1975) and is loosely bracketed up to 15 GPa (Katsura and Ito, 1990). For $CaCO_3$, the melting curve is constrained up to 21 GPa (Li et al., 2017; Suito et al., 2001). Incongruent melting of calcite and magnesite has been suggested below 0.7 and 2.3 GPa, respectively (Irving and Wyllie, 1975; Huang and Wyllie, 1976). At higher pressures Ca–Mg carbonates are supposed to melt congruently (Shatskiy et al., 2018; Buob, 2006), but the occurrence of periclase in experimental studies on the Na_2CO_3–$MgCO_3$-$CaCO_3$ system at 6 GPa (Shatskiy et al., 2016; Podborodnikov et al., 2018) and on the Na_2CO_3–$MgCO_3$ system at 3 GPa calls the melting relations into question.

Here, we extend the known $CaCO_3$–$MgCO_3$ melting relations to 9 GPa and argue for incongruent melting of Mg-rich carbonates producing periclase at pressures between 4 and 9 GPa. Periclase is sometimes found only in high-resolution transmission electron microscopy (TEM) images, implying that previous studies may have missed small periclase grains in experimental run products. Furthermore, we determine partition coefficients between Ca-magnesite and dolomitic melt and between Mg-calcite and dolomitic melt at 9 GPa, extending our previous results at 6 GPa (Sieber et al., 2020). The trace element signature of dolomitic melt in equilibrium with Ca-magnesite and periclase could be used to approximate CO_2-rich liquids parental to kimberlite magmas.

2 Experimental setup

Table 1 gives an overview of the experimental conditions. Starting mixtures (labeled CM5–CM9) consist of milled natural or synthetic magnesite and laboratory-grade, synthetic $CaCO_3$ establishing molar Mg proportions ($X_{Mg} = Mg/(Mg + Ca)$) of 0.1, 0.2, 0.45 and 0.85 (Table 1). Natural magnesite with 0.7 ± 0.1 wt % FeO, 0.35 ± 0.05 wt % MnO and 0.18 ± 0.5 wt % CaO from Brumado, Brazil, was used in the mixtures CM7–CM9, and synthetic magnesite ($MgCO_3$) was used in CM5–CM6. Minor quantities of laboratory-grade Li, Na, K, Ba and Sr carbonates; Pb, Nb and Y oxides; and rare earth elements (REEs) as oxides (purities $\geq$ 99.9 %, except for La_2O_3 with a purity of 94 %) were added into the starting mixtures, establishing concentrations listed in Table S1 (Supplement). The bulk compositions of the starting materials were analyzed on cold-pressed pellets of the starting mixtures.

Ground starting mixtures were dried at $\sim$ 120 °C for several days to minimize adsorption of water before being loaded in cold-sealed Pt capsules. Experiments at 9 GPa and between 1450 to 1800 °C were performed using a 14/8 assembly, a Re foil as the heater and a $LaCrO_3$ jacket (Fig. 1a). A double-stepped graphite heater and ZrO_2 jacket were used in experiments at 1300 °C (run 121, 9 GPa) and in run 133 at 6 GPa (Fig. 1b). The latter were performed in an 18/11 assembly. All experiments were performed in a Walker-type multi-anvil press at the GFZ German Research Centre for Geosciences. Temperature was monitored throughout the run with a type-C thermocouple (WRe5%–WRe26% wires) surrounded by BN powder to create reduced conditions preventing temporal drift of the measured temperature (Watenphul et al., 2009). Run durations were 6 h, except for experiments performed at the highest and lowest temperatures (Table 1). The press was rotated 180° on its axis at 5° s^{-1} because continuous mixing of the liquid and solid phase promotes equilibrium (Schmidt and Ulmer, 2004). Rotation was started after compression and before heating. Steady rotation was stopped only 0.5 min before power to the heater was turned

off. Run 121 conducted at the lowest investigated temperature (1300 °C) was run for 168 h but without rotation.

To test the melting reaction using an approach previously followed by Huang and Wyllie (1976), run 150 (9 GPa, 1600 °C, CM5) was performed in excess of CO_2. To ensure CO_2 saturation, a small inner Pt capsule containing the starting material (CM5) was enclosed by a larger Pt capsule containing Ag-oxalate (Fig. 1c). The inner capsule was closed but not sealed. Ag-oxalate was synthesized from solutions of Ag-nitrate and oxalic acid. Ag-oxalate formed a deposit that was air-dried and stored in a desiccator for several days before being loaded into the experimental cargo. Ag-oxalate decomposes upon heating, producing ~ 15 wt % CO_2 in the bulk composition. The released Ag is alloyed with the metal of the capsules, minimizing contamination of the experimental charge.

Two additional samples were kindly provided by Jan Müller (sample MA 507) and Hans-Josef Reichmann (sample MA 523). Both samples contained only magnesite and were earlier performed to investigate the melting point of magnesite under high pressure at the GFZ. MA 507 was run at 6 GPa and 1775 °C for 2 h and MA 523 at 4 GPa and 1770 °C for only 2 min (Table 1). Here we report unpublished TEM images and measurement of these samples to discuss the melting reactions (see Discussion).

3 Analytical methods

After the multi-anvil experiments, the recovered capsules were mounted in epoxy and polished.

Raman spectroscopy (HORIBA Jobin Yvon LabRAM HR 800) was used for phase identification and to ensure the absence of hydrous phases. Raman spectra over a spectral range of 100–1200 and 3000–4000 cm^{-1} were accumulated over 20 s using an Nd:YAG (532 nm) laser with a 50× objective lens.

Quantitative wavelength-dispersive spectrometry (WDS) was performed on C-coated mounts using a field-emission electron probe micro-analyzer (FE-EPMA; JEOL SuperProbe JXA-8230). Laser ablation inductively coupled plasma mass spectrometry (LA-ICP-MS) was carried out using the Analyte Excite 193 nm ArF* excimer-based laser ablation system (Teledyne Photon Machines, Bozeman, MT, USA), coupled to the quadrupole ICP-MS iCAP from Thermo Scientific. Spot sizes were varied depending on grain size. Quenched melt and cold-pressed pellets of the starting mixtures were measured with a defocused beam with a diameter of 40 µm (FE-EPMA) and 50 µm (LA-ICP-MS). Measurements details and chemical data are available in the open-access data publication of Sieber et al. (2022).

TEM measurements on samples MA 507 and MA 523 were performed on a FEI Tecnai G2 F20 X-Twin transmission electron microscope and a FEI FIB200TEM focused ion beam (FIB) device for specimen preparation (Wirth, 2004).

Table 1. Experimental run conditions and molar $Mg/(Mg + Ca) = X_{Mg}$ ratios are listed.

Run	Pressure	Temperature	Start	X_{Mg} start	Duration	Run products			X^{carb}_{Mg}	ΔX^{carb}_{Mg}	X^{carb}_{Mg}	ΔX^{carb}_{Mg}	X^{liq}_{Mg}	ΔX^{liq}_{Mg}
						Carbonate crystal	Carbonate liquid	Periclase						
no.	[GPa]	[°C]	material	material	[h]									
run 112	9	1500	CM6	0.10	6	×	×	×	0.056	0.002			0.12	0.003
run 111	9	1600	CM9	0.20	6		×	×					0.133	0.007
run 121	9	1300	CM9	0.20	168	×	×		0.155	0.004			0.26	0.01
run 120	9	1450	CM8	0.45	6	×	×		0.84	0.01	0.51	0.03	0.35	0.01
run 149	9	1450	CM8	0.45	6	×	×		0.84	0.03	0.545	0.008	0.30	0.01
run 109	9	1500	CM5	0.85	6	×	×	×	0.961	0.008			0.48	0.01
run 110	9	1600	CM5	0.85	6	×	×	×	0.96	0.01			0.65	0.01
run 150	9	1600	CM5	0.85	6	×	×		0.989	0.003			0.85	0.02
run 151	9	1600	CM5	0.85	6	×	×	×	0.963	0.003			0.70	0.08
run 115	9	1800	CM7	0.85	5 h 15 min		×	×					0.831	0.003
run 116	9	1700	CM7	0.85	1 h 18 min	×	×	×	0.960	0.003			0.75	0.05
run 133	6	1500	CM5	0.85	6	×			0.921	0.007			0.56	0.06
MA 507	6	1775	$MgCO_3$	1	2		×	×						
MA 523	4	1700	$MgCO_3$	1	2 min		×	×						

Abbreviations: carb, carbonate crystal; liq, liquid; X is the $Mg/(Mg + Ca)$ molar ratio.

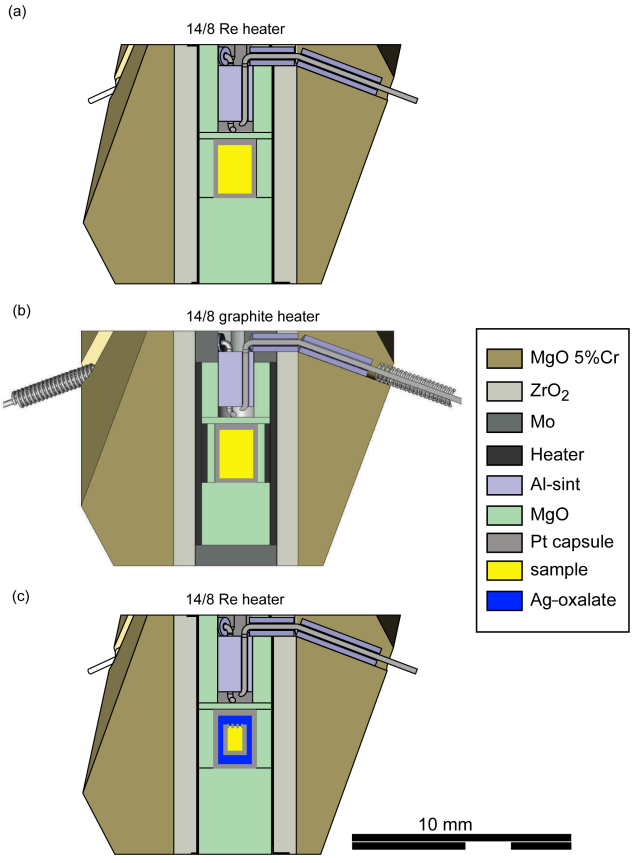

Figure 1. Technical drawing of experimental setup: **(a)** 14/8 Re heater (run 112, 111, 120, 149, 109, 110, 151, 115, 116), **(b)** 14/8 graphite heater (run 121, 133), and **(c)** 14/8 Re heater with an inner capsule containing the start material and an outer capsule containing Ag-oxalate to establish CO_2 (run 150).

Chemical compositions were analyzed by energy-dispersive X-ray (EDX) spectroscopy. Crystal structures were characterized by fast Fourier transform (FFT) diffraction patterns from high-resolution transmission electron microscopy (HREM) images.

4 Results

4.1 Textures and composition of post-run phases

All experiments were conducted above the solidus because quenched liquid is always present. The quenched carbonate melt forms dentritic aggregates and contains small bubbles, indicating the presence of a vapor phase (Fig. 2). Post-run assemblies contain quenched liquid and carbonate and periclase crystals (Table 1). At temperatures above the liquidus, only quenched carbonate melt and rounded periclase crystals are observed (run 111, 115; Table 1).

Liquid accumulates at the hottest part of the capsule, which is located close to the thermocouple in experiments using Re foil as the heater (Fig. 2a, b) and in the center of the capsule in experiments using a double-stepped graphite heater (Fig. 2c). Small amounts of liquid are also trapped between euhedral carbonate crystals (Fig. 2d, e). Anhedral and rounded periclase grains are mostly contained within the liquid fraction (Fig. 2d–f), but some periclase grains are adjacent to carbonates (Fig. 2d, e).

The textures of experiments interpreted to have been conducted near the solidus (run 120, 149, 121) are somewhat different, and overall equilibrium may not be reached (see Discussion). Using CM8 at 1450 °C (run 120, 149), a layered texture is present with carbonate melt ($X_{Mg} = 0.35 \pm 0.01$) at the bottom, Ca-bearing magnesite ($X_{Mg} = 0.83 \pm 0.01$) in the middle and carbonates of intermediate Ca–Mg composition at the top of the capsule. The composition of these carbonates varies from Mg-rich ($X_{Mg} = 0.59$) at the contact with magnesite grains to Mg-poor ($X_{Mg} = 0.41$) at the top of the capsule. Liquid is trapped within the solid carbonates, with the amount of interstitial melt decreasing from the magnesite zone toward the top of the capsule. This zonation is interpreted to have developed at high temperature as it is present in both run 120, which was quenched shortly after the press stopped rotating, and run 149, which was quenched during rotation.

Using starting material CM9 at 1300 °C, run 121 was performed near the solidus. Three zones are distinguishable (Fig. 2c): first, Mg-calcite with $X_{Mg} = 0.155 \pm 0.004$ forms a structure across the capsule reminiscent of the letter "X"; second, carbonate grains of different compositions and with grain sizes between 20 and 100 µm are present in the upper and lower parts of the X; and third, quenched liquid with $X_{Mg} = 0.26 \pm 0.01$ is present at each side of the X. In the backscatter electron (BSE) images, small contrast differences appear between the upper and lower parts of the X-structured Mg-calcite, suggesting a different composition. Nevertheless, the X-structured Mg-calcite is chemically homogenous within the uncertainty in FE-EPMA and LA-ICP-MS measurements. In the upper part of the capsule, the carbonate grains have X_{Mg} values of either 0.26 ± 0.01 or 0.16 ± 0.003 and are indistinguishable within the uncertainty from carbonates in the lower part, which have X_{Mg} values of 0.27 ± 0.01 and 0.156 ± 0.003. The centers of some Ca-richer carbonate grains contain calcite with variable Mg content ($X_{Mg} = 0.10 \pm 0.08$). In some grains, the Mg content of Mg-rich carbonates decreases from the center to the rim of the grains.

4.2 Phase relations

The $CaCO_3$–$MgCO_3$ system between 6 and 9 GPa can be described by the six phases aragonite, Mg-calcite, dolomite, Ca-magnesite, periclase and melt. Depending on the X_{Mg} of the starting material, Mg-calcite (CM6, CM9), Ca-magnesite (CM5, CM7), or dolomite and Ca-magnesite (CM8) appear as carbonate phases according to Raman spectroscopy

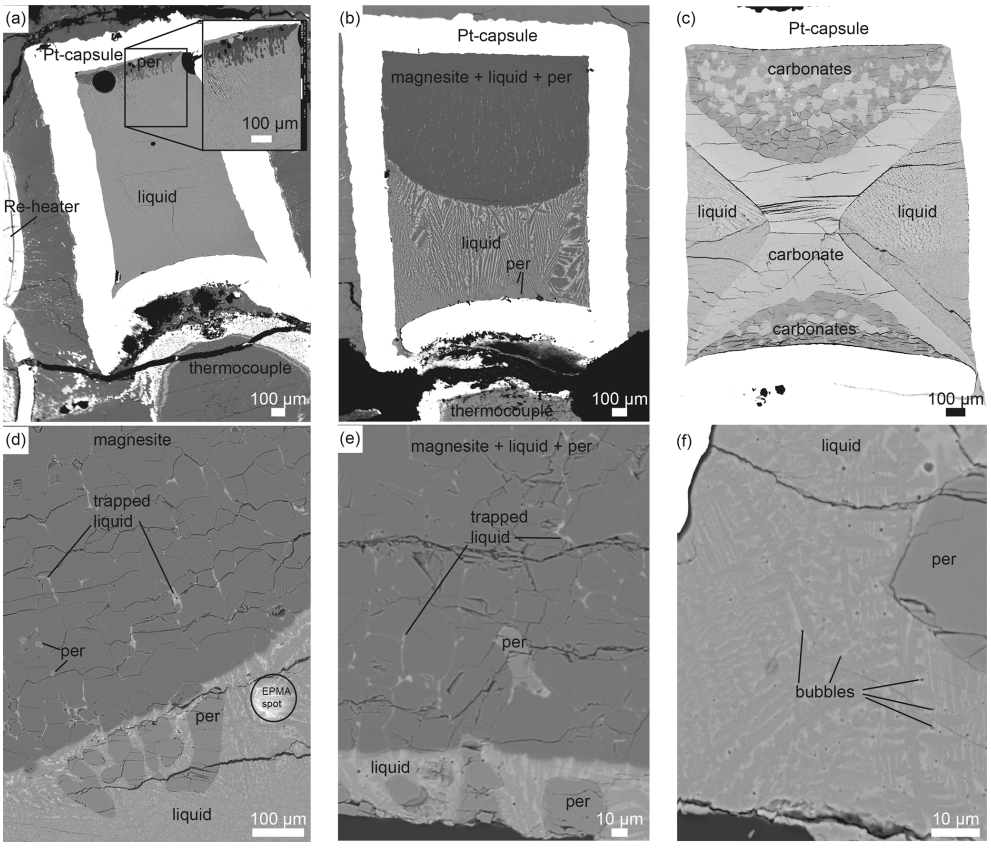

Figure 2. BSE images of run products: **(a)** run 115; **(b)** run 116; **(c)** run 121; **(d)** run 109; **(e, f)** run 110. Abbreviation: per, periclase.

(Fig. 3). Aragonite was not observed because it can incorporate only a limited amount of Mg, e.g., 5 mol % $MgCO_3$ at 6 GPa (Shatskiy et al., 2018). Extrapolation of the reaction curve aragonite + dolomite = Mg-calcite studied by Hermann et al. (2016) up to 6.5 GPa and 950 °C confirms the presence of Mg-calcite. Further, Mg-calcite was reported at 6 GPa by Shatskiy et al. (2018) and Müller et al. (2017).

Figure 4 summarizes the sub- and supra-solidus phase relations in the $CaCO_3$–$MgCO_3$-system between 1 and 9 GPa after Byrnes and Wyllie (1981), Sieber et al. (2020), Shatskiy et al. (2018), Irving and Wyllie (1975), and this study. Byrnes and Wyllie (1981) and Irving and Wyllie (1975) investigated the subsolidus and melting relations of the $CaCO_3$–$MgCO_3$-system at 1 and 3 GPa, respectively. Byrnes and Wyllie (1981) corrected the pressure of Irving and Wyllie (1975) later by 10 % to 2.7 GPa. Since Irving and Wyllie (1975) conducted experiments for only 1 to 3 min, the liquidus temperatures could be overestimated. The duration to generate melt might be too short to generate detectable amounts of melt in quenched experiments. Figure 4 shows a truly binary join only at 2.7 GPa because ternary fields exist at 1, 6 and 9 GPa (see Discussion).

Between 1 and 9 GPa, the general geometries of stability boundaries are invariable (Fig. 4). At 1 GPa, the eutectic

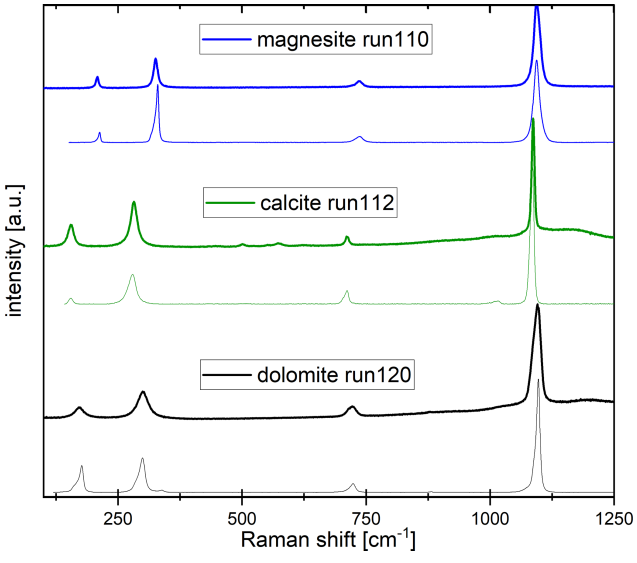

Figure 3. Raman spectra (bold lines) of unoriented magnesite (run 110), calcite (run 112) and dolomite (run 120) displayed together with RRUFF reference spectra (thin lines; https://rruff.info/, last access: November 2020) of magnesite (R040114), calcite (R040170) and dolomite (R050357), respectively.

point is at $X_{Mg} = 0.32$ and 1075 °C. From 2.7 to 6 and 9 GPa the eutectic point shifts marginally and lies at $X_{Mg} = 0.42$ and 1290 °C, $X_{Mg} = 0.37$ and 1260 °C, and $X_{Mg} = 0.28$ and 1260 °C, respectively. The melting points of the end-members magnesite and calcite increase by around 400 and 200 °C, respectively, extending the stability field of carbonate + melt with increasing pressure. On the Ca-rich side of the eutectic point, Mg-calcite coexists with liquid and periclase. The stability field of calcite + liquid + periclase narrows with increasing temperature, and X_{Mg} of Mg-calcite and liquid decreases. The melting point of pure calcite at 9 GPa is 1740 °C (Li et al., 2017).

The peritectic point lies at the Mg-rich join of the eutectic point and shifts with increasing pressure from $X_{Mg} = 0.36$ and 1125 °C (1 GPa) to $X_{Mg} = 0.48$ and 1380 °C (2.7 GPa) to $X_{Mg} = 0.44$ and 1360 °C (6 GPa) to $X_{Mg} = 0.35$ and 1450 °C (9 GPa) (Fig. 4). The range in X_{Mg} between the eutectic and peritectic point expands with increasing pressure, enlarging the stability field of dolomite + melt. At 9 GPa, dolomite could be stable over a temperature range from ∼ 1260 to ∼ 1450 °C. The dolomite–magnesite solvus at ∼ 1450 °C produces the peritectic reaction: dolomite → magnesite + liquid. On the Mg-rich side of the peritectic point, Ca-magnesite coexists with periclase and carbonate melt. This stability field is much larger in terms of X_{Mg} than the narrower stability field of Mg-calcite + liquid + periclase. The composition of Ca-magnesite varies marginally along the phase boundary, but the X_{Mg} of the carbonate melt increases considerably with increasing temperature, so the phase field of liquid + periclase diminishes with increasing temperature. The melting point of pure magnesite at 9 GPa is not known. For reference, we plot the melting point of magnesite at 8 GPa (2000 °C; Katsura and Ito, 1990). The 6 GPa experiment confirms the earlier established phase relations (Fig. 4b) (Sieber et al., 2020).

4.3 Trace element composition and distribution

Carbonate melts contain between 0.1 wt % and 2.4 wt % SiO_2 and less than 0.2 wt % Al_2O_3, with the highest content in experiments using CM5 and CM6 (see data publication – Sieber et al., 2022). Ca-rich carbonate melts ($X_{Mg} = 0.12$ to 0.26) are enriched in Li, Na, K, Ba, Y and REEs by 2 to 8 times relative to the starting material (run 112, 121). In comparison, the enrichment of trace elements is more pronounced in the Mg-rich carbonate melt. For example, under the same *PT* conditions, the Mg-rich carbonate melt ($X_{Mg} = 0.48$ to 0.65) is enriched 2 to 14 times in Y and REEs and 11 to 22 times in Li, Na and K compared to the starting material (run 109, 110). The Pt used as capsule material is soluble to some extent in carbonate melt, so carbonate melts contain small amounts of Pt (< 7 ppm). The concentration of Pt in the carbonate melt is constant across the capsule, indicating that the melt was sufficiently mixed; otherwise a diffusion profile would have been expected. The concentration of Pt in carbonate melt increases with temperature from < 1 ppm at ≤ 1600 °C to 7 ppm at 1800 °C (Sieber et al., 2022). Some elements such as Fe, Ni and Pb are alloyed with the Pt of the capsule. The concentrations of trace elements in periclase crystals are below the LA-ICP-MS detection limit (Sieber et al., 2022).

In chemical equilibrium and according to Henry's law, the distribution of an element between two phases is independent of its concentration. The ratio between the concentrations (c) of a trace element (i) in two phases, which here are a solid (s) and a liquid (l) phase, is defined as the Nernst partition coefficient (D):

$$^{s/l}D_i = \frac{^{s}c_i}{^{l}c_i}.$$

Partition coefficients are given in Table 2. Mg-calcite contains small amounts of Li, Na and K, giving partition coefficients between 0.04 and 0.19 (run 121). Mn, Fe, Sr and Pb are moderately compatible in Mg-calcite, with partition coefficients ranging from 0.45 to 2.3 (Fig. 6a). Heavy REEs (Gd to Lu) show partition coefficients just below 1 (D_{HREE} between 0.95 and 0.74). With increasing ionic radii, the REE content in Mg-calcite decreases and partition coefficients of light REEs (La to Eu) range from 0.8 to 0.5 (Fig. 6a).

Ca-magnesite crystals are incompatible for singly charged cations because the concentrations of Li, Na and K in Ca-magnesite are below the LA-ICP-MS detection limit (Sieber et al., 2022). Sr and Ba are moderately incompatible ($D_{Sr} = 0.006$ to 0.02; $D_{Ba} = 0.01$ to 0.02) in Ca-magnesite grains ($X_{Mg} = 0.96$) occurring with carbonate melt ($X_{Mg} = 0.48$ to 0.75) (Fig. 6b). Carbonate melts in equilibrium with Ca-magnesite and periclase grains show strong fractionation from heavy to light REEs (Fig. 6b), which is much lower for carbonate melt coexisting with Mg-calcite crystals (Fig. 6a).

5 Discussion

5.1 Approach to equilibrium

Several lines of evidence point toward chemical equilibrium. The major and trace element composition of single carbonate grains is homogeneous and uniform between individual grains of the same experiment. Likewise, the major and trace element composition of the liquid is homogeneous across the capsule, and liquid trapped between carbonate crystals has the same major element composition as liquid elsewhere in the capsule. Further, equilibrium is supported as triple junctions between homogenous carbonate crystals can be observed (Hunter and McKenzie, 1989). The multi-anvil press was rotated throughout the entire run (stopping the rotation 30 s before quenching), enhancing equilibrium between solids and a mobile phase (Schmidt and Ulmer, 2004). Our earlier experiments investigating the same chemical system

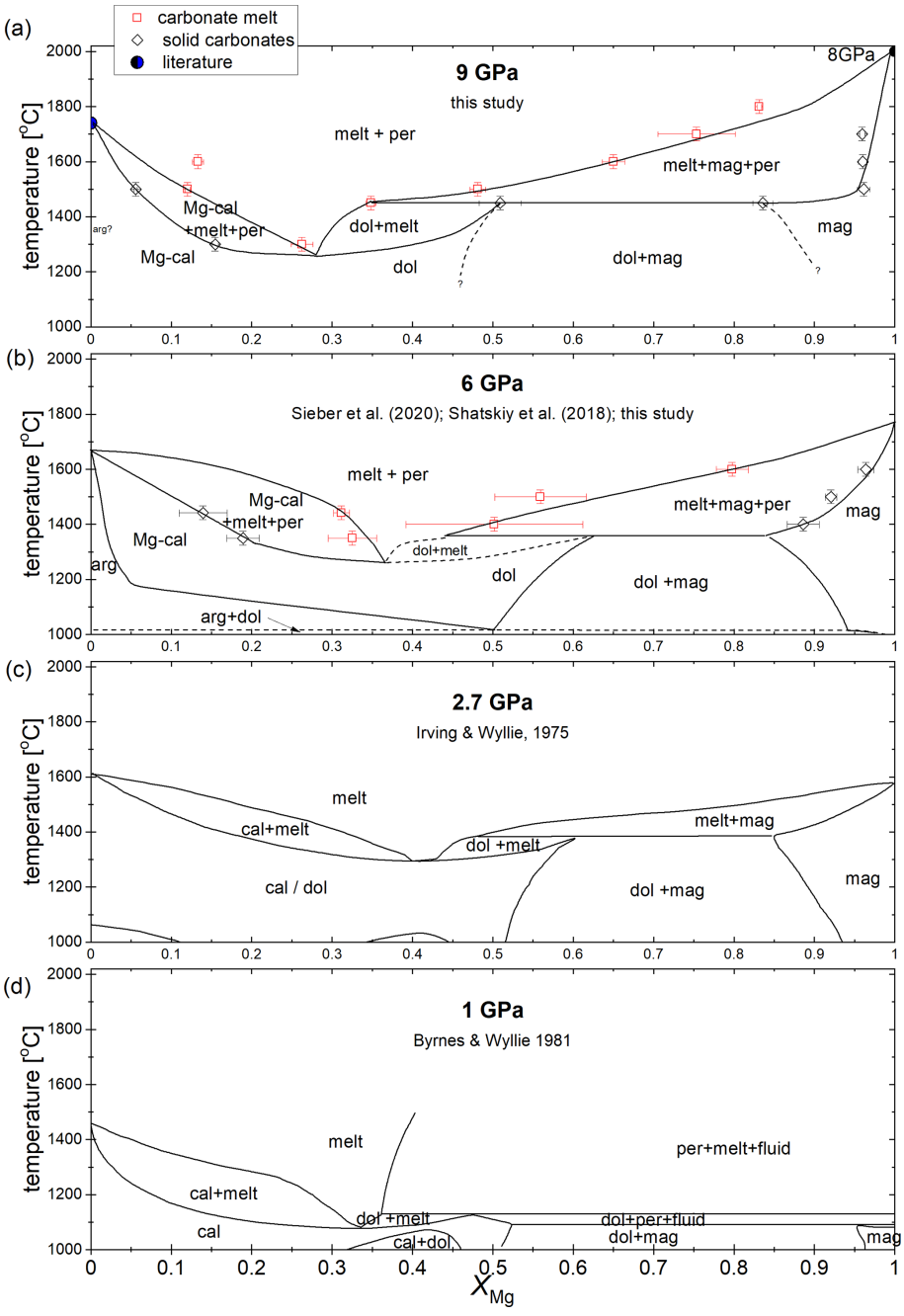

Figure 4. Phase relations in the $CaCO_3$–$MgCO_3$ system at **(a)** 9 GPa, **(b)** 6 GPa, **(c)** 2.7 GPa and **(d)** 1 GPa; Abbreviations: arg, aragonite; cal, calcite; dol, dolomite; mag, magnesite; per, periclase.

in the same matter also point toward equilibrium (Sieber et al., 2020).

Overall equilibrium seems to have been hampered in experiments (run 120, 149, 121) performed close to the solidus. A thermal gradient in run 121 with the hottest part in the middle of the capsule may explain the observed X-shape texture (Fig. 3c) (Johnson and Walker, 1993). Most liquid is located at the hottest part of the capsule (center of the capsule) and might here be in equilibrium with solids. At the colder parts of the capsule, equilibrium had to be established via solid-state diffusion, which was not completed within 6 h as implied by the compositional variation of carbonate grains.

5.2 Melting reactions and periclase formation

Below we discuss the timing and consequences of periclase formation. The role of periclase in carbonatitic rocks is crit-

ical as periclase in carbonatites may form by incongruent melting of dolomite in the presence of water (Chakhmouradian et al., 2016) or as a breakdown reaction of dolomite (Stoppa et al., 2019). However, previous studies on carbonate phase relationships at high pressures have made ambiguous observations on the melting reactions of carbonates and the possible associated formation of periclase. These ambiguous observations, described below, make it necessary to determine the timing of periclase formation in our experiments. Periclase may have been present at the start of the experiment when it was introduced by the starting mixtures as small impurities of the natural magnesite, or periclase may have formed at high pressure and temperature along with the liquid and carbonate grains, or periclase crystals represent a quench phase. In our previous study on the melting relations of Ca–Mg carbonates at 6 GPa, we speculated that periclase was introduced as an impurity from the natural magnesite used in the starting material. This hypothesis can now be ruled out because X-ray diffraction (XRD) of the powdered natural sample showed only magnesite reflections and because periclase grains are also found in experiments with synthetic $MgCO_3$ in the starting mixtures (CM5, CM6).

Calcite melts incongruently at pressures below 0.7 GPa and $\sim 1375\,^{\circ}C$ (Irving and Wyllie, 1975; Huang and Wyllie, 1976; Byrnes and Wyllie, 1981) in Reaction (R1):

$$\text{calcite (s)} = \text{liquid} + CO_2\ \text{(f)}, \tag{R1}$$

with s and f referring to a solid and fluid phase, respectively. At higher pressure, calcite melts congruently (Irving and Wyllie, 1975; Huang and Wyllie, 1976).

The presence of periclase and vapor was noted at 1 GPa for the dolomite–magnesite join of the $CaCO_3$–$MgCO_3$ system (Byrnes and Wyllie, 1981). In the MgO–CO_2 system, the dissociation curve of magnesite (magnesite = periclase + CO_2) terminates at an invariant point at ~ 2.3 GPa and $\sim 1550\,^{\circ}C$ where magnesite begins to melt incongruently up to 2.7 GPa and 1590 °C via Reaction (R2) (Huang and Wyllie, 1976):

$$\text{magnesite (s)} = \text{liquid} + \text{periclase (s)}. \tag{R2}$$

At higher pressure (≥ 2.7 GPa), congruent melting is suggested (Huang and Wyllie, 1976). No periclase crystals are reported in experimental studies of melting relations in the $CaCO_3$–$MgCO_3$ system (Müller et al., 2017) and in the K_2CO_3–$CaCO_3$–$MgCO_3$ system (Shatskiy et al., 2016) at 6 GPa. Melting of magnesite at 8 GPa and 2000 °C has been reported to produce a magnesite melt without periclase (Katsura and Ito, 1990).

In contrast, periclase crystals and bubbles were observed in most experiments performed above the solidus at 6 and 9 GPa. Periclase forms in both Mg- and Ca-rich bulk compositions (Table 1). Periclase grains exist in the quenched liquid and between solid carbonate grains (Fig. 2). If periclase crystals were to separate from the melt upon quenching, we would expect them to be found only in liquid-rich areas, have small crystal sizes and be uniformly distributed in the liquid, which is not the case. Moreover, the comparison between run 110 and 150 using the same starting material and *PT* conditions confirms that periclase is a stable phase formed in an incongruent melting reaction. In run 150, CO_2 saturation was established at the beginning of the experiment by adding Ag-oxalate into an outer capsule (Fig. 1c). Periclase grains formed in run 110 but not in run 150. Small and sometimes euhedral periclase crystals have also been reported along with magnesite grains and carbonate liquid for Na-poor bulk compositions in the Na_2CO_3–$MgCO_3$–$CaCO_3$ system at 6 GPa and in the Na_2CO_3–$MgCO_3$ system at 3 GPa (Podborodnikov et al., 2018; Shatskiy et al., 2016). In these studies, the occurrence of periclase was attributed to partial disproportioning of $MgCO_3$ just above the solidus.

In summary, we conclude that periclase grains coexist with carbonate melt and carbonate crystals at high pressure, making the $CaCO_3$–$MgCO_3$ system a pseudo-binary system as the number of components increases. This result calls into question the existence of a singular point reported by Huang and Wyllie (1976) at which magnesite melts congruently. The discrepancy with some previous experimental studies could be explained by short run times of a few minutes, which are probably not sufficient to reach equilibrium (Huang and Wyllie, 1976) or/and because small grains of periclase might have been overlooked. For example, Müller et al. (2017) did not observe any periclase using the microprobe, but recent TEM studies of their sample (MA 507, 6 GPa, 1775 °C, 2 h) show the presence of fine-grained periclase grains between magnesite melts (Fig. 5a). Similarly, melting of $MgCO_3$ at 4 GPa, 1700 °C and 2 min (MA 523) resulted in small periclase grains as shown by TEM studies (Fig. 5b, d).

5.3 Trace element partitioning

Solid–liquid partition coefficients depend on a number of factors such as pressure, temperature, oxygen fugacity, and the composition and structure of melt and crystal. The main difference in the trigonal $R\bar{3}c$ crystal structures of calcite and magnesite is that the distortion of the CaO_6 octahedron in calcite is larger than that of MgO_6 in magnesite (Effenberger et al., 1981). Based on our experiments, it is not possible to constrain the contribution of the extensive and intensive parameters to the partition coefficients. However, some general observations observed in all experiments are made.

The crystal–chemical control over the incorporation of trace elements and consequently over mineral–melt partitioning can be described by lattice-site elastic-strain models (Onuma et al., 1968; Nagasawa, 1966; Beattie, 1994; Blundy and Wood, 2003). Accordingly, the logarithms of the partition coefficient for a specific site in the crystal vary in a quasi-parabolic trend with the radius of the substituting cation. Figure 6 displays such a quasi-parabolic relationship fitted with the equation given by Blundy and Wood (2003). Cation radii in 6-fold coordination are taken from Shannon

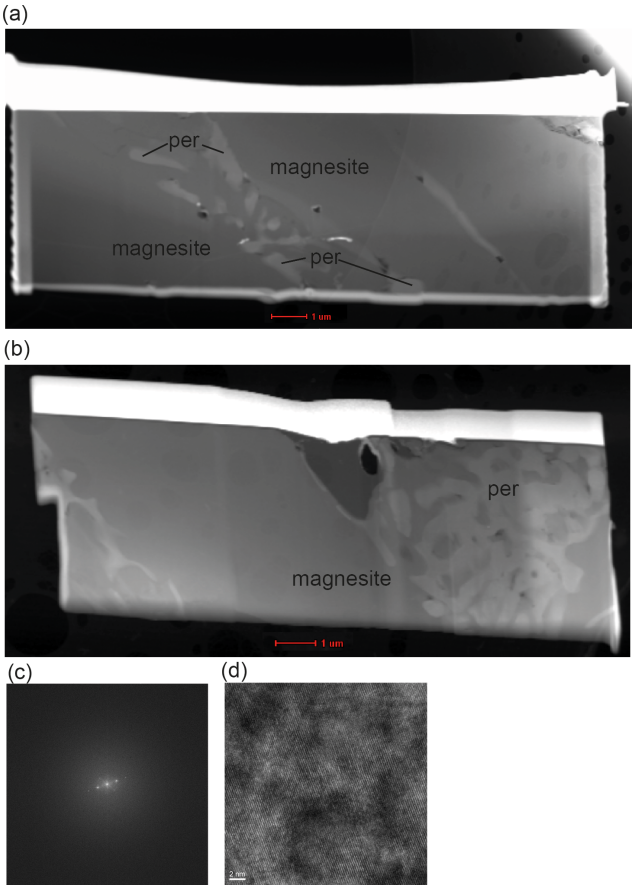

Figure 5. Overviews of FIB foils, sample MA 507 **(a)** and MA 523 **(b)**; **(c)** FFT diffraction pattern of periclase from HREM image **(d)** of sample MA 523.

and Prewitt (1970). The fitted parameters are listed in Table S2. Consistent with the lattice-site elastic-strain model, the partition coefficients for divalent cations decrease following a parabolic trend with increasing difference from the radii of $^{[6]}Ca^{2+}$ for Mg-calcite (Fig. 6a) and $^{[6]}Mg^{2+}$ for Ca-magnesite (Fig. 6b). Accordingly, $^{[6]}Fe^{2+}$ and $^{[6]}Mn^{2+}$ are more compatible in Ca-magnesite than the larger $^{[6]}Sr^{2+}$, $^{[6]}Pb^{2+}$ and $^{[6]}Ba^{2+}$ (Fig. 6b). It also follows that the partition coefficient of $^{[6]}Sr^{2+}$, $^{[6]}Pb^{2+}$ and $^{[6]}Ba^{2+}$ between Mg-calcite and carbonate melt decreases as the cation radii increase (Fig. 6a).

A charge compensation mechanism must occur for any heterovalent substitution. With a similar ionic radius to $^{[6]}Ca^{2+}$, the singly charged $^{[6]}Na^{+}$ may substitute for $^{[6]}Ca^{2+}$ in Mg-calcite, and $^{[6]}Na^{+}$ is more compatible in Mg-calcite than the smaller $^{[6]}Li^{+}$ and larger $^{[6]}K^{+}$ (Fig. 6a). Na in Ca-magnesite is below the LA-ICP-MS detection limit. Tri-valent rare earth elements (REEs) $^{[6]}Y^{3+}$ and $^{[6]}Al^{3+}$ may substitute for $^{[6]}Mg^{2+}$ in Mg-calcite and in Ca-magnesite because the partition coefficient increases as the ionic radii approach the radius of $^{[6]}Mg^{2+}$. For Mg-calcite, this may indicate coupled substitution, with single charged cations occupying the $^{[6]}Ca^{2+}$ position and tri-valent cations occupying the $^{[6]}Mg^{2+}$ position. Experimental studies of the distribution of trace element between an aqueous solution and calcite, as well as theoretical considerations from the perspective of electron orbital and bonding types, indicate that actinides and lanthanides, when present in trace amounts, occupy $^{[6]}Ca^{2+}$ sites in Mg-poor to Mg-free calcite (Zhong and Mucci, 1995; Lakshtanov and Stipp, 2004; Elzinga et al., 2002; Stipp et al., 2006). Zhong and Mucci (1995) reported incorporation of Na^{+} from seawater-like solutions into calcite being correlated with the incorporation of REE^{3+} and concluded that REE^{3+} substitute on the $^{[6]}Ca^{2+}$ site and that Na^{+} may compensate for the tri-valent charge of REEs. However, the influence of pressure, temperature and Mg content on the substitution mechanism of tri-valent REEs into calcite remains unconstrained, but the ability of calcite to incorporate lanthanides may increase with pressure and temperature. For example, experiments at ambient conditions and with Eu^{3+} as a representative lanthanide have shown that calcite can incorporate about 0.06 mol % Eu^{3+} (Stipp et al., 2006), but the ability of calcite to incorporate La^{3+} is about 9 times higher at 0.7 GPa and 1200 °C (Biedermann, 2020).

In contrast to calcite, Ca-magnesite can host much smaller quantities of lanthanides. The greater abundance of larger CaO_6 octahedra in Mg-calcite compared to Ca-magnesite may favor the incorporation of lanthanides, especially light REEs, with similar cation radii to Ca^{2+}. The partition coefficients of heavy REEs such as $^{[6]}Lu^{3+}$ ($D_{Lu} = 0.05$ to 0.18) between Ca-magnesite and dolomitic melt are 16–9 times higher compared to D_{La}. Thus, melting of Mg-rich carbonates leads to a dolomitic melt with strong fractionation between heavy and light REEs.

It should be noted that the applicability of the lattice-site elastic-strain models is limited because the ionic radii under high pressure are unknown and the models do not account for the influence of melt composition and structure.

6 Implications and conclusions

The melting relations of the nominally anhydrous $CaCO_3$–$MgCO_3$ system were studied at 6 and 9 GPa in multi-anvil experiments, using the rocking mode to improve chemical equilibrium. We conclude that Ca–Mg carbonates (partially) melt at 9 GPa for temperatures above 1260 °C. The eutectic melting temperature is marginally affected by pressure between 6 and 9 GPa. Considering the thermal structure of subduction zones (Syracuse et al., 2010), Ca–Mg carbonates within the subducting slab are stable up to 9 GPa. Carbonate-rich melts will be produced atop a subducting slab or by diapiric rise of carbonate-bearing lithologies into the mantle wedge.

Our study shows incongruent melting of Ca–Mg carbonates to periclase and carbonate melt for pressures above

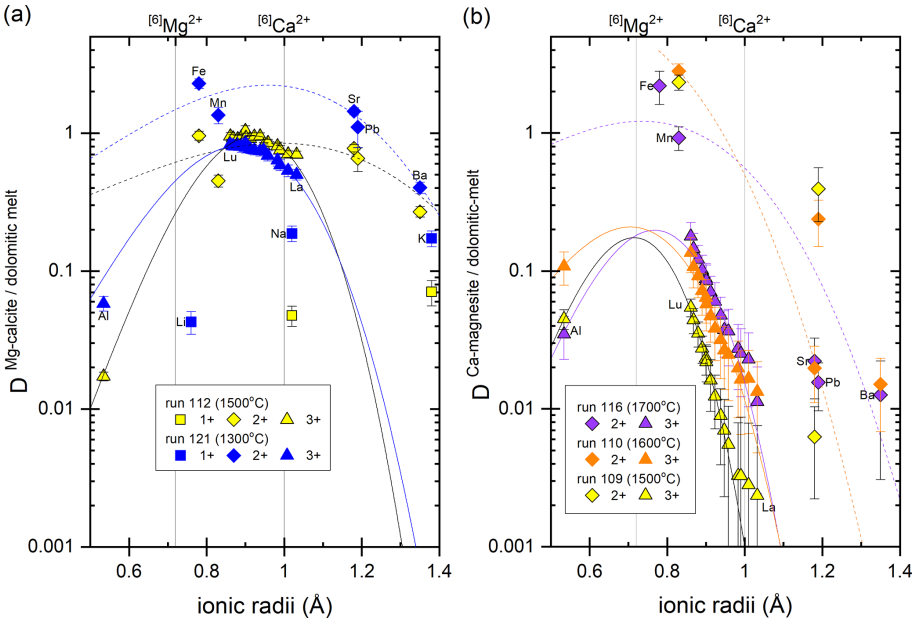

Figure 6. Partition coefficient at 9 GPa as a function of ionic radii for **(a)** Mg-calcite and carbonate melt (run 112, 121) and **(b)** Ca-magnesite and carbonate melt (run 116, 110, 109).

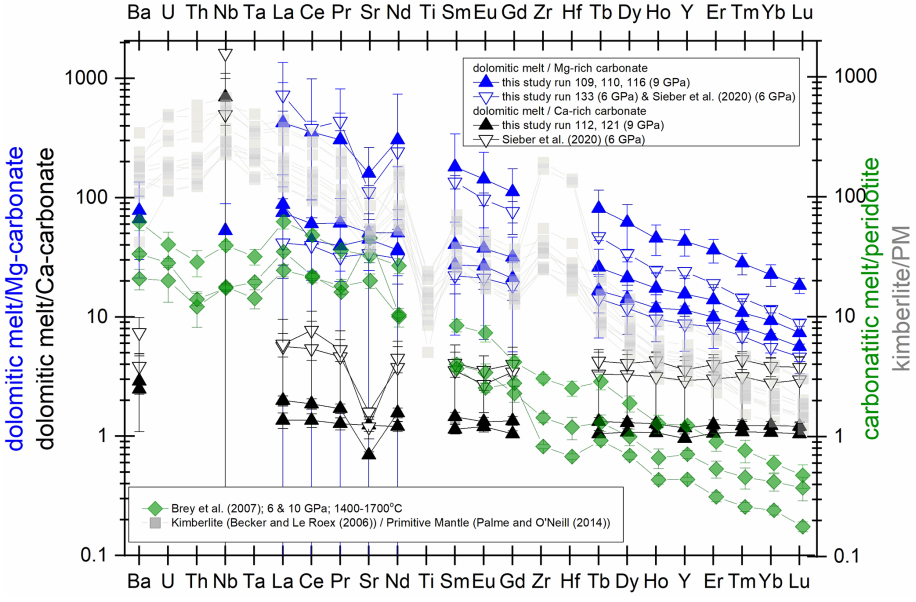

Figure 7. Trace element signature in the pure carbonate system (blue: Mg-rich composition; black: Ca-rich composition) compared to carbonatitic melt/peridotite (Brey et al., 2007) and Group-I kimberlites (Becker and Le Roex, 2006) normalized to the primitive mantle (Palme and O'Neill, 2014). Note that the strong fractionation of heavy to light REEs of primitive kimberlitic melts can be approached by our melting experiments at 9 GPa and at 6 GPa with Ca-magnesite and dolomitic melt.

Table 2. Partition coefficients.

Run	112		121		109		110		116		133	
	D	ΔD	D	ΔD	D	ΔD	D	ΔD	D	ΔD	D	ΔD
Li			0.043	0.008								
Na	0.048	0.008	0.19	0.02								
Mg	0.45	0.02	1.2	0.1	4.0	0.2	4.0	0.3	1.0	0.2	1.5	0.4
Al	0.017	0.001	0.058	0.007	0.045	0.007	0.11	0.03	0.03	0.01	0.23	0.07
Si												
P	0.29	0.04	0.49	0.08								
K	0.07	0.01	0.17	0.02								
Ca	1.06	0.03	2.3	0.1	0.16	0.02	0.21	0.03	0.16	0.01	0.20	0.05
Cr			0.6	0.1							1.8	0.6
Mn	0.45	0.05	1.3	0.2	2.3	0.3	2.8	0.4	0.93	0.18	1.2	0.4
Fe	0.96	0.07	2.3	0.2					2.2	0.6	4.9	1.7
Sr	0.78	0.05	1.44	0.09	0.006	0.004	0.02	0.01	0.02	0.01	0.03	0.03
Y	1.04	0.09	0.85	0.06	0.023	0.006	0.06	0.02	0.09	0.03	0.11	0.05
Nb			0.0014	0.0006					0.02	0.01		
Ba	0.27	0.02	0.40	0.04			0.02	0.01	0.01	0.01		
La	0.70	0.04	0.50	0.05	0.002	0.005	0.013	0.009	0.011	0.009	0.02	0.03
Ce	0.70	0.04	0.53	0.05	0.003	0.005	0.02	0.01	0.02	0.01	0.03	0.04
Pr	0.76	0.06	0.59	0.05	0.003	0.005	0.02	0.01	0.03	0.01	0.03	0.04
Nd	0.81	0.05	0.64	0.06	0.003	0.005	0.02	0.01	0.03	0.01	0.03	0.04
Sm	0.85	0.05	0.69	0.06	0.006	0.005	0.02	0.01	0.04	0.02	0.05	0.03
Eu	0.81	0.05	0.75	0.06	0.007	0.005	0.03	0.01	0.04	0.01	0.05	0.03
Gd	0.95	0.06	0.74	0.06	0.009	0.005	0.03	0.02	0.05	0.02	0.05	0.04
Tb	0.95	0.06	0.75	0.06	0.012	0.005	0.04	0.02	0.06	0.02	0.07	0.04
Dy	0.91	0.05	0.77	0.06	0.016	0.007	0.05	0.02	0.07	0.02	0.08	0.03
Ho	0.93	0.06	0.79	0.07	0.022	0.006	0.06	0.02	0.09	0.03	0.10	0.04
Er	0.94	0.06	0.80	0.07	0.027	0.006	0.07	0.02	0.10	0.03	0.12	0.04
Tm	0.91	0.06	0.82	0.07	0.035	0.007	0.09	0.03	0.12	0.03	0.14	0.05
Yb	0.92	0.05	0.81	0.06	0.044	0.009	0.11	0.03	0.15	0.04	0.18	0.06
Lu	0.95	0.06	0.83	0.07	0.054	0.008	0.14	0.04	0.18	0.05	0.22	0.06
Pb	0.7	0.1	1.1	0.3	0.4	0.2	0.24	0.09	0.02	0.01	0.04	0.03

4 GPa, suggesting an alternative formation mechanism of periclase in carbonatitic rocks. In natural systems, elevated iron or silica activities may favor the precipitation of Mg-rich magnetite or Mg-silicates, respectively, instead of periclase, explaining the rarity of periclase in carbonatites (Reguir et al., 2008; Barker, 2001).

CO_2-rich melts produced by very low-degree melting of a Ca-magnesite-bearing mantle are considered the precursor of more evolved carbonatitic and kimberlitic magmas (Jones et al., 2013; Yaxley et al., 2019, and references therein). Precise determinations of the trace element composition of experimental near-solidus melts are limited due to their small proportions. Brey et al. (2007, 2009, 2011) studied partial melting of carbonated peridotites by loading a peridotite–carbonate mixture into a natural olivine container, which then was sealed into a Pt capsule. Their unique experimental setup allowed small amounts of melt to be extracted from the peridotite matrix. Thus, the element content of even small amounts of melt could be analyzed without contamination by the solids. A time series performed by Brey et al. (2007) showed that the initial melt of a magnesite-bearing peridotite contains less than 3 wt % SiO_2 and small amounts of Al_2O_3 (0.1 wt %), but the trace element compositions could only be established in experiments with higher degrees of partial melting (melts containing 10 wt %–20 wt % SiO_2 and 0.2 wt % to 0.5 wt % Al_2O_3). Here, carbonate melts contain less than 0.2 wt % Al_2O_3 and 0.4 ± 0.1 wt % SiO_2 (run 116, CM7) or ~ 2 wt % SiO_2 (run 109, 110, 133; CM5), which is similar to the initial melt reported by Brey et al. (2007). Interestingly, the strong fractionation of heavy to light REEs in those experiments mimics the REE signature of Group-I kimberlites taken from Becker and Roex (2006) (Fig. 7). This implies that the Mg-rich join of the carbonate system might be a good analogue to model the REE signature of near-solidus melts of magnesite-bearing peridotites. However, a carbonated lherzolite may contain 0.02 wt %–0.2 wt % magnesite (Dasgupta and Hirschmann, 2006); such small magnesite proportions will make a limited contribution to the trace element content and signature of carbonatitic and kimberlitic

melts, and the main silicate minerals have to be considered (Dasgupta et al., 2009; Girnis et al., 2013).

Data availability. Data are available open access in Sieber et al. (2022, https://doi.org/10.5880/GFZ.3.6.2022.001).

Supplement. The supplement related to this article is available online at: https://doi.org/10.5194/ejm-34-411-2022-supplement.

Author contributions. MJS performed and analyzed the experiments and wrote the manuscript. MW and MKM contributed to the discussion and understanding of the experimental results. OA and MO performed the electron microprobe and LA-ICP-MS measurements, respectively. MKM had the initial idea for the project.

Competing interests. The contact author has declared that none of the authors has any competing interests.

Disclaimer. Publisher's note: Copernicus Publications remains neutral with regard to jurisdictional claims in published maps and institutional affiliations.

Acknowledgements. The authors are grateful to Andreas Ebert and Christoph Möller for their assistance in experimental and analytical work. Rita Luchitskaia (Goethe University, Frankfurt) is thanked for magnesite synthesis. Special thank to Jan Müller and Hans-Josef Reichmann for providing samples and Richard Wirth and Anja Schreiber for FIB foils and TEM measurements of those samples. We further thank Francesco Stoppa and the anonymous reviewer for constructive comments and Elisabetta Rampone and Stefano Poli for editorial handling of the manuscript.

Financial support. This study was funded by the DFG-funded research group FOR 2125 CarboPaT under the grant number KO1260/19-1 and supported within the funding program "Open-Access-Publikationskosten" of the Deutsche Forschungsgemeinschaft (DFG, German Research Foundation) – project number 491075472.

The article processing charges for this open-access publication were covered by the Helmholtz Centre Potsdam – GFZ German Research Centre for Geosciences.

Review statement. This paper was edited by Stefano Poli and reviewed by Francesco Stoppa and one anonymous referee.

References

Barker, D. S.: Calculated silica activities in carbonatite liquids, Contrib. Mineral. Petr., 141, 704–709, https://doi.org/10.1007/s004100100281, 2001.

Beattie, P.: Systematics and energetics of trace-element partitioning between olivine and silicate melts: Implications for the nature of mineral/melt partitioning, Chem. Geol., 117, 57–71, https://doi.org/10.1016/0009-2541(94)90121-x, 1994.

Becker, M. and Le Roex, A. P. L.: Geochemistry of South African on-and off-craton, Group I and Group II kimberlites: petrogenesis and source region evolution, J. Petrol., 47, 673–703, https://doi.org/10.1093/petrology/egi089, 2006.

Biedermann, N.: Carbonate-silicate reactions at conditions of the Earth's mantle and the role of carbonates as possible trace-element carriers, PhD thesis, 2020.

Blundy, J. and Wood, B.: Partitioning of trace elements between crystals and melts, Earth Planet. Sci. Lett., 210, 383–397, https://doi.org/10.1016/s0012-821x(03)00129-8, 2003.

Brenker, F. E., Vollmer, C., Vincze, L., Vekemans, B., Szymanski, A., Janssens, K., Szaloki, I., Nasdala, L., Joswig, W., and Kaminsky, F.: Carbonates from the lower part of transition zone or even the lower mantle, Earth Planet. Sc. Lett., 260, 1–9, 2007.

Brey, G. P., Bulatov, V. K., Girnis, A. V., and Lahaye, Y.: Experimental Melting of Carbonated Peridotite at 6–10 GPa, J. Petrol., 49, 797–821, https://doi.org/10.1093/petrology/egn002, 2007.

Brey, G. P., Bulatov, V. K., and Girnis, A. V.: Influence of water and fluorine on melting of carbonated peridotite at 6 and 10 GPa, Lithos, 112, 249–259, https://doi.org/10.1016/j.lithos.2009.04.037, 2009.

Brey, G. P., Bulatov, V. K., and Girnis, A. V.: Melting of K-rich carbonated peridotite at 6–10 GPa and the stability of K-phases in the upper mantle, Chem. Geol., 281, 333–342, https://doi.org/10.1016/j.chemgeo.2010.12.019, 2011.

Buob, A.: Experiments on $CaCO_3$-$MgCO_3$ solid solutions at high pressure and temperature, Am. Mineral., 91, 435–440, https://doi.org/10.2138/am.2006.1910, 2006.

Byrnes, A. P. and Wyllie, P. J.: Subsolidus and melting relations for the join $CaCO_3$-$MgCO_3$ at 10 kbar, Geochim. Cosmochim. Ac., 45, 321–328, https://doi.org/10.1016/0016-7037(81)90242-8, 1981.

Chakhmouradian, A. R., Reguir, E. P., and Zaitsev, A. N.: Calcite and dolomite in intrusive carbonatites. I. Textural variations, Mineral. Petrol., 110, 333–360, 2016.

Dalton, J. A. and Presnall, D. C.: The Continuum of Primary Carbonatitic-Kimberlitic Melt Compositions in Equilibrium with Lherzolite: Data from the System CaO-MgO-Al_2O_3-SiO_2-CO_2 at 6 GPa, J. Petrol., 39, 1953–1964, https://doi.org/10.1093/petroj/39.11-12.1953, 1998.

Dasgupta, R. and Hirschmann, M. M.: Melting in the Earth's deep upper mantle caused by carbon dioxide, Nature, 440, 659–662, https://doi.org/10.1038/nature04612, 2006.

Dasgupta, R. and Hirschmann, M. M.: The deep carbon cycle and melting in Earth's interior, Earth Planet. Sci. Lett., 298, 1–13, https://doi.org/10.1016/j.epsl.2010.06.039, 2010.

Dasgupta, R., Hirschmann, M. M., McDonough, W. F., Spiegelman, M., and Withers, A. C.: Trace element partitioning between garnet lherzolite and carbonatite at 6.6 and 8.6 GPa with applications to the geochemistry of the man-

tle and of mantle-derived melts, Chem. Geol., 262, 57–77, https://doi.org/10.1016/j.chemgeo.2009.02.004, 2009.

Effenberger, H., Mereiter, K., and Zemann, J.: Crystal structure refinements of magnesite, calcite, rhodochrosite, siderite, smithonite, and dolomite, with discussion of some aspects of the stereochemistry of calcite type carbonates, Z. Krist.-Cryst. Mater., 156, 233–243, https://doi.org/10.1524/zkri.1981.156.14.233, 1981.

Elzinga, E., Reeder, R., Withers, S., Peale, R. E., Mason, R., Beck, K. M., and Hess, W. P.: EXAFS study of rare-earth element coordination in calcite, Geochim. Cosmochim. Ac., 66, 2875–2885, https://doi.org/10.1016/S0016-7037(02)00888-8, 2002.

Falloon, T. J. and Green, D. H.: The solidus of carbonated, fertile peridotite, Earth Planet. Sc. Lett., 94, 364–370, https://doi.org/10.1016/0012-821X(89)90153-2, 1989.

Ghosh, S., Ohtani, E., Litasov, K. D., and Terasaki, H.: Solidus of carbonated peridotite from 10 to 20 GPa and origin of magnesiocarbonatite melt in the Earth's deep mantle, Chem. Geol., 262, 17–28, https://doi.org/10.1016/j.chemgeo.2008.12.030, 2009.

Girnis, A. V., Bulatov, V. K., Brey, G. P., Gerdes, A., and Höfer, H. E.: Trace element partitioning between mantle minerals and silico-carbonate melts at 6–12 GPa and applications to mantle metasomatism and kimberlite genesis, Lithos, 160–161, 183–200, https://doi.org/10.1016/j.lithos.2012.11.027, 2013.

Hammouda, T. and Keshav, S.: Melting in the mantle in the presence of carbon: Review of experiments and discussion on the origin of carbonatites, Chem. Geol., 418, 171–188, https://doi.org/10.1016/j.chemgeo.2015.05.018, 2015.

Hermann, J., Troitzsch, U., and Scott, D.: Experimental subsolidus phase relations in the system $CaCO_3$–$CaMg(CO_3)_2$ up to 6.5 GPa and implications for subducted marbles, Contrib. Mineral. Petr., 171, 84, https://doi.org/10.1007/s00410-016-1296-y, 2016.

Huang, W.-L. and Wyllie, P. J.: Melting relationships in the systems CaO-CO_2 and MgO-CO_2 to 33 kilobars, Geochim. Cosmochim. Ac., 40, 129–132, https://doi.org/10.1016/0016-7037(76)90169-1, 1976.

Humphreys, E. R., Bailey, K., Hawkesworth, C. J., Wall, F., Najorka, J., and Rankin, A. H.: Aragonite in olivine from Calatrava, Spain—Evidence for mantle carbonatite melts from > 100 km depth, Geology, 38, 911–914, https://doi.org/10.1130/g31199.1, 2010.

Hunter, R. H. and McKenzie, D.: The equilibrium geometry of carbonate melts in rocks of mantle composition, Earth Planet. Sc. Lett., 92, 347–356, https://doi.org/10.1016/0012-821x(89)90059-9, 1989.

Ionov, D. A., Dupuy, C., O'Reilly, S. Y., Kopylova, M. G., and Genshaft, Y. S.: Carbonated peridotite xenoliths from Spitsbergen: implications for trace element signature of mantle carbonate metasomatism, Earth Planet. Sc. Lett., 119, 283–297, https://doi.org/10.1016/0012-821X(93)90139-Z, 1993.

Irving, A. J. and Wyllie, P. J.: Subsolidus and melting relationships for calcite, magnesite and the join $CaCO_3$-$MgCO_3$ 36 kb, Geochim. Cosmochim. Ac., 39, 35–53, https://doi.org/10.1016/0016-7037(75)90183-0, 1975.

Johnson, M. C. and Walker, D.: Brucite [MG(OH)2] dehydration and the molar volume of H_2O to 15 GPa, Am. Mineral., 78, 271–284, 1993.

Jones, A. P., Genge, M., and Carmody, L.: Carbonate Melts and Carbonatites, Rev. Mineral. Geochem., 75, 289–322, https://doi.org/10.2138/rmg.2013.75.10, 2013.

Katsura, T. and Ito, E.: Melting and subsolidus phase relations in the $MgSiO_3MgCO_3$ system at high pressures: implications to evolution of the Earth's atmosphere, Earth Planet. Sc. Lett., 99, 110–117, https://doi.org/10.1016/0012-821x(90)90074-8, 1990.

Korsakov, A. V. and Hermann, J.: Silicate and carbonate melt inclusions associated with diamonds in deeply subducted carbonate rocks, Earth Planet. Sc. Lett., 241, 104–118, https://doi.org/10.1016/j.epsl.2005.10.037, 2006.

Lakshtanov, L. and Stipp, S.: Experimental study of europium (III) coprecipitation with calcite, Geochim. Cosmochim. Ac., 68, 819–827, https://doi.org/10.1016/j.gca.2003.07.010, 2004.

Li, Z., Li, J., Lange, R., Liu, J., and Militzer, B.: Determination of calcium carbonate and sodium carbonate melting curves up to Earth's transition zone pressures with implications for the deep carbon cycle, Earth Planet. Sc. Lett., 457, 395–402, https://doi.org/10.1016/j.epsl.2016.10.027, 2017.

Litasov, K. D.: Physicochemical conditions for melting in the Earth's mantle containing a C–O–H fluid (from experimental data), Russ. Geol. Geophys., 52, 475–492, https://doi.org/10.1016/j.rgg.2011.04.001, 2011.

Müller, J., Koch-Müller, M., Rhede, D., Wilke, F. D. H., and Wirth, R.: Melting relations in the system $CaCO_3$-$MgCO_3$ at 6 GPa, Am. Mineral., 102, 2440–2449, https://doi.org/10.2138/am-2017-5831, 2017.

Nagasawa, H.: Trace element partition coefficient in ionic crystals, Science, 152, 767–769, https://doi.org/10.1126/science.152.3723.767, 1966.

Onuma, N., Higuchi, H., Wakita, H., and Nagasawa, H.: Trace element partition between two pyroxenes and the host lava, Earth Planet. Sc. Lett., 5, 47–51, https://doi.org/10.1016/S0012-821X(68)80010-X, 1968.

Palme, H. and O' Neill, H.: Cosmochemical Estimates of Mantle Composition, Treatise on Geochemistry, 2nd Edn., 3, 1–39, https://doi.org/10.1016/B978-0-08-095975-7.00201-1, 2014.

Podborodnikov, I. V., Shatskiy, A., Arefiev, A. V., Chanyshev, A. D., and Litasov, K. D.: The system Na_2CO_3–$MgCO_3$ at 3 GPa, High Pressure Res., 38, 281–292, https://doi.org/10.1080/08957959.2018.1488972, 2018.

Reguir, E. P., Chakhmouradian, A. R., Halden, N. M., Yang, P., and Zaitsev, A. N.: Early magmatic and reaction-induced trends in magnetite from the carbonatites of Kerimasi, Tanzania, Can. Mineral., 46, 879–900, https://doi.org/10.3749/canmin.46.4.879, 2008.

Schmidt, M. W. and Ulmer, P.: A rocking multianvil: elimination of chemical segregation in fluid-saturated high-pressure experiments, Geochim. Cosmochim. Ac., 68, 1889–1899, https://doi.org/10.1016/j.gca.2003.10.031, 2004.

Shannon, R. and Prewitt, C.: Revised values of effective ionic radii, Acta Crystallogr. B, 26, 1046–1048, https://doi.org/10.1107/S0567740870003576, 1970.

Shatskiy, A., Sharygin, I. S., Gavryushkin, P. N., Litasov, K. D., Borzdov, Y. M., Shcherbakova, A. V., Higo, Y., Funakoshi, K.-I., Palyanov, Y. N., and Ohtani, E.: The system K_2CO_3-$MgCO_3$ at 6 GPa and 900–1450 °C, Am. Mineral., 98, 1593–1603, https://doi.org/10.2138/am.2013.4407, 2013.

Shatskiy, A., Litasov, K. D., Sharygin, I. S., Egonin, I. A., Mironov, A. M., Palyanov, Y. N., and Ohtani, E.: The system Na_2CO_3–$CaCO_3$–$MgCO_3$ at 6 GPa and 900–1250 °C and its relation to the partial melting of carbonated mantle, High Pressure Research, 36, 23–41, https://doi.org/10.1080/08957959.2015.1135916, 2016.

Shatskiy, A., Podborodnikov, I. V., Arefiev, A. V., Minin, D. A., Chanyshev, A. D., and Litasov, K. D.: Revision of the $CaCO_3$–$MgCO_3$ phase diagram at 3 and 6 GPa, Am. Mineral., 103, 441–452, https://doi.org/10.2138/am-2018-6277, 2018.

Shatsky, V., Ragozin, A., and Sobolev, N.: Some aspects of metamorphic evolution of ultrahigh-pressure calc-silicate rocks of the Kokchetav Massif, Russ. Geol. Geophys., 47, 105–119, 2006.

Sieber, M. J., Wilke, F., and Koch-Müller, M.: Partition coefficients of trace elements between carbonates and melt and suprasolidus phase relation of Ca-Mg-carbonates at 6 GPa, Am. Mineral., 105, 922–931, https://doi.org/10.2138/am-2020-7098, 2020.

Sieber, M. J., Wilke, F. D. H., Appel, O., Oelze, M., and Koch-Müller, M.: Major and trace element analysis of Ca-Mg-carbonates and carbonate melt at 6 and 9 GPa, V.1, GFZ Data Services [data set], https://doi.org/10.5880/GFZ.3.6.2022.001, 2022.

Stipp, S. L. S., Christensen, J. T., Lakshtanov, L. Z., Baker, J. A., and Waight, T. E.: Rare Earth element (REE) incorporation in natural calcite: Upper limits for actinide uptake in a secondary phase, Radiochim. Acta, 94, 523–528, https://doi.org/10.1524/ract.2006.94.9-11.523, 2006.

Stoppa, F., Schiazza, M., Rosatelli, G., Castorina, F., Sharygin, V. V., Ambrosio, F. A., and Vicentini, N.: Italian carbonatite system: From mantle to ore-deposit, Ore Geol. Rev., 114, 103041, https://doi.org/10.1016/j.oregeorev.2019.103041, 2019.

Suito, K., Namba, J., Horikawa, T., Taniguchi, Y., Sakurai, N., Kobayashi, M., Onodera, A., Shimomura, O., and Kikegawa, T.: Phase relations of CaCO3at high pressure and high temperature, Am. Mineral., 86, 997–1002, https://doi.org/10.2138/am-2001-8-906, 2001.

Syracuse, E. M., van Keken, P. E., and Abers, G. A.: The global range of subduction zone thermal models, Phys. Earth Planet. In., 183, 73–90, https://doi.org/10.1016/j.pepi.2010.02.004, 2010.

Wallace, M. E. and Green, D. H.: An experimental determination of primary carbonatite magma composition, Nature, 335, 343–346, https://doi.org/10.1038/335343a0, 1988.

Wang, A., Pasteris, J. D., Meyer, H. O. A., and Dele-Duboi, M. L.: Magnesite-bearing inclusion assemblage in natural diamond, Earth Planet. Sc. Lett., 141, 293–306, https://doi.org/10.1016/0012-821x(96)00053-2, 1996.

Watenphul, A., Wunder, B., and Heinrich, W.: High-pressure ammonium-bearing silicates: Implications for nitrogen and hydrogen storage in the Earth's mantle, Am. Mineral., 94, 283–292, https://doi.org/10.2138/am.2009.2995, 2009.

Wirth, R.: Focused Ion Beam (FIB): A novel technology for advanced application of micro- and nanoanalysis in geosciences and applied mineralogy, Eur. J. Mineral., 16, 863–876, https://doi.org/10.1127/0935-1221/2004/0016-0863, 2004.

Yaxley, G. M. and Brey, G. P.: Phase relations of carbonate-bearing eclogite assemblages from 2.5 to 5.5 GPa: implications for petrogenesis of carbonatites, Contrib. Mineral. Petr., 146, 606–619, https://doi.org/10.1007/s00410-003-0517-3, 2004.

Yaxley, G. M. and Green, D. H.: Experimental demonstration of refractory carbonate-bearing eclogite and siliceous melt in the subduction regime, Earth Planet. Sc. Lett., 128, 313–325, https://doi.org/10.1016/0012-821x(94)90153-8, 1994.

Yaxley, G. M., Ghosh, S., Kiseeva, E. S., Mallik, A., Spandler, C., Thomson, A. R., and Walter, M. J.: CO_2-Rich Melts in Earth, in: Deep Carbon: Past to Present, edited by: Orcutt, B. N., Daniel, I., and Dasgupta, R., Cambridge University Press, Cambridge, 129–162, https://doi.org/10.1017/9781108677950, 2019.

Zedgenizov, D. A., Kagi, H., Shatsky, V. S., and Ragozin, A. L.: Local variations of carbon isotope composition in diamonds from São-Luis (Brazil): Evidence for heterogenous carbon reservoir in sublithospheric mantle, Chem. Geol., 363, 114–124, https://doi.org/10.1016/j.chemgeo.2013.10.033, 2014.

Zhong, S. and Mucci, A.: Partitioning of rare earth elements (REEs) between calcite and seawater solutions at 25 °C and 1 atm, and high dissolved REE concentrations, Geochim. Cosmochim. Ac., 59, 443–453, https://doi.org/10.1016/0016-7037(94)00381-U, 1995.